CFD ANALYSIS OF TURBULENT MIXED CONVECTION UPWARD FLOW OF SUPERCRITICAL WATER IN A VERTICAL TUBE

Vladimir Agranat
Applied Computational Fluid Dynamics Analysis
Thornhill, Ontario, Canada
vlad@acfda.org

Michael Malin
Concentration, Heat & Momentum Limited
Wimbledon, London, United Kingdom
mrm@cham.co.uk

Rand Abdullah, Igor Pioro
University of Ontario Institute of Technology
Oshawa, Ontario, Canada
Rand.Abdullah@uoit.ca, Igor.Pioro@uoit.ca

ABSTRACT

A Computational Fluid Dynamics (CFD) model is developed for the prediction of heat transfer to supercritical water (SCW) flowing upwards in vertical tubes under the conditions of turbulent mixed convection. The model is validated using experimental data obtained under the operating conditions typical for SCW cooled reactors (SCWRs), namely: at a pressure of 24 MPa, an inner tube diameter of 10 mm, an inlet temperature of 320 or 350 °C and a heated tube length of 4 m. Four values of the mass flux (200, 500, 1000 and 1500 kg/m^{2}s) and various values of the wall heat flux (ranging from 129 to 729 kW/m^2) are considered. The physical properties of SCW are calculated by using the REFPROP software from National Institute of Standards and Technology (NIST). The model has been incorporated into the commercial general-purpose CFD software, PHOENICS. Various turbulence models and numerical grid settings are tested. The study has demonstrated a good agreement between the CFD predictions and the experimental data on the inside tube wall temperature and heat transfer coefficient with use of a two-layer low-Reynolds-number k-ε turbulence model and a proper numerical grid spacing. However, this good agreement deteriorates appreciably under the influence of strong buoyancy forces at the lowest mass flux value of 200 kg/m^{2}s. Further research is required to improve the model's performance under these conditions. Practical recommendations are made regarding potential model applications in 3D analyses of SCWRs.

KEYWORDS

CFD, Supercritical Water, Heat Transfer, Vertical Tube, Upward Flow, PHOENICS

1. INTRODUCTION

Nuclear energy is considered a reliable, powerful and environmentally-friendly source for electricity generation in the world in the coming years compared to fossil-fuelled power plants and renewable sources of energy such as wind and solar. However, current Nuclear Power Plants (NPPs), especially, equipped with water-cooled reactors, have relatively low gross thermal efficiencies (30-36%) compared to those of advanced thermal power plants (55-62%). Therefore, there is a need to develop new nuclear reactors with inherent safety and higher thermal efficiencies in order to increase electricity generation per kilogram of fuel and decrease detrimental effects on the environment. To address these issues a number

of countries worldwide are developing next generation or Generation-IV nuclear-reactor concepts (six in total) and, as a result, NPPs will have significantly higher operating parameters, especially, temperatures (550-1000°C). Also, Generation-IV nuclear technology will include SuperCritical-Pressure (SCP) reactor coolants (helium and water) and/or SCP working fluids in power cycles (carbon dioxide, helium and water). Due to this the reliable and accurate prediction methods for heat transfer in SuperCritical Fluids (SCFs) should be developed and verified. These methods include: empirical correlations, Computational Fluid Dynamics (CFD) predictions, and use of special-purpose Thermal-Hydraulics codes.

For more than 40 years, CFD [1] has been increasingly used as a predictive tool in the analyses of supercritical water (SCW) heat transfer in vertical upward and downward tube flows. Compared to empirical 1-D correlations, CFD studies allow to look inside the flow and to have a better picture of various phenomena related to heat transfer in SCFs.

The standard modern practice is to apply the commercial general-purpose CFD codes (FLUENT, ANSYS-CFX, PHOENICS, etc.) for such analyses. Numerous researchers have assessed FLUENT and ANSYS-CFX for SCW heat transfer modeling with use of different turbulence models and grid settings. Some recent applications of these codes are described in [2-7]. In particular, a detailed review [3] of CFD applications to the modeling of SCW heat transfer in vertical tube flows described the advances and shortcomings in this field. No universal turbulent model has been proposed yet in order to enable researchers to predict accurately SCW heat transfer for a wide range of operating conditions along the whole heated tube length.

In this paper, a CFD model based on customizing the PHOENICS CFD software [8] is developed and partially validated using the experimental database on SCW heat transfer in a 4-m bare vertical tube (D=10 mm) with upward flow under operating conditions typical for SCWRs [9-12]. CFD predictions of the inside tube wall temperatures and Heat Transfer Coefficients (HTCs) were compared with measurements. The results show that the PHOENICS CFD model can predict experimental HTC values reasonably well under some operating conditions, but under other conditions, especially within a Deteriorated-Heat-Transfer (DHT) regime, disagreement may possibly appear between the experimental data and the CFD results. In general, HTCs in a bare tube can be considered as a conservative approach in predicting minimum possible HTCs in more complex geometries such as bundles.

2. MATHEMATICAL MODEL

2.1. Mean-flow equations: The mean-flow equations for a statistically steady turbulent flow are:

$$\nabla.(\rho\mathbf{U}) = 0 \qquad (1)$$

$$\nabla.(\rho\mathbf{U}\otimes\mathbf{U}) = -\nabla p + (\rho - \rho_r)\mathbf{g} + \nabla.\left(\rho(\nu+\nu_t)\left[\nabla U + \nabla U^T\right]\right) \qquad (2)$$

$$\nabla.(\rho\mathbf{U}h) = \nabla.\left(\left[k_l + k_t\right]\nabla\mathrm{T}\right); \qquad h = \int_{T_0}^{T} C_p dT \qquad (3)$$

where ρ is the fluid density, **U** is the velocity vector, ν and ν_t are the molecular and turbulent kinematic viscosities, p is the relative pressure, ρ_r is the reference density, **g** is the gravitational vector, the superscript T denotes that the transpose of the dyadic is taken, T is the absolute temperature, k_l and k_t are the molecular and turbulent thermal conductivities, h is the specific enthalpy, C_p is the thermodynamic specific heat, i.e. it is the differential rate of variation of enthalpy with temperature at constant pressure, and T_0 is a given reference temperature.

2.2. Turbulence Model: The turbulent viscosity and turbulent conductivity are determined from the two-layer k-ε model of Rodi [13], which uses the standard high-Re k-ε model away from the wall and the one-equation k-l_m model near the wall to resolve the near-wall viscosity-affected layer, as follows:

$$\nabla.(\rho \mathbf{U} k) = \nabla.(\rho[\nu + \nu_t / \sigma_k]\nabla k) + \rho(P_k - \varepsilon) \tag{4}$$

$$\nabla.(\rho \mathbf{U} \varepsilon) = \nabla.(\rho[\nu + \nu_t / \sigma_\varepsilon]\nabla \varepsilon) + \rho\varepsilon(c_{1\varepsilon} P_k - c_{2\varepsilon}\varepsilon)/k \tag{5}$$

$$\nu_t = c_\mu c_d k^2 / \varepsilon; \quad k_t = \rho\nu_t C_p / \sigma_t; \quad P_k = \nu_t\left(\nabla \mathbf{U} + (\nabla \mathbf{U})^T\right):\nabla \mathbf{U} \tag{6}$$

where the model coefficients are $c_\mu c_d$=0.09, σ_k=1.0, σ_ε=1.314, $c_{1\varepsilon}$=1.44 and $c_{2\varepsilon}$=1.92, and σ_t is the turbulent Prandtl number. The effect of σ_t on CFD predictions of SCW heat transfer in the upward tube flows has been investigated in [6], but here a uniform value of σ_t=0.86 [14] is used for all cases, unless stated otherwise. Although the buoyancy force is taken into account in the momentum equation (2), its direct effect on the turbulence field is ignored in equations (4) and (5).

In the near-wall layer, the two-layer model fixes the dissipation rate ε, which appears in the k equation, to:

$$\varepsilon = c_d k^{3/2} f_2 / l_m; \quad f_2 = 1. + 5.3/\mathrm{Re}_n; \quad \mathrm{Re}_n = k^{1/2} y_n / \nu; \quad l_m = \kappa y_n \tag{7}$$

where c_d=0.1643, von Karman's constant κ=0.41, f_2 is a damping function, l_m is Prandtl's mixing length, and y_n is the minimum distance to the nearest wall. The turbulent kinematic viscosity in the near-wall layer is calculated from:

$$\nu_t = f_\mu c_\mu k^{1/2} l_m; \quad f_\mu = \left(1 - e^{(-0.0198\,\mathrm{Re}_n)}\right) \tag{8}$$

where c_μ=0.5478 and f_μ is another damping function. The one-equation model is matched with the high-Re k-ε model at those locations where Re_n= 350.

2.3. Physical properties: The physical properties of supercritical water, namely density, kinematic viscosity, specific heat at constant pressure and thermal conductivity vary dramatically with temperature approaching pseudo-critical conditions, and tabulated values are calculated by the NIST REFPROP software [15] at the specified operating pressure of 24MPa, and temperature range of 320°C to 600°C.

3. SOLUTION METHOD

3.1. Flow geometry and conditions: The case considered is vertical upward flow in a cylindrical tube with an inner diameter of 10 mm and a heated tube length of 4 m under various operating conditions [9-11]. A cylindrical-polar coordinate system (X, Y, Z) is used to represent flow geometry, and the flow is presumed two-dimensional with axial symmetry. The sizes of the computational domain in the radial and axial directions are 5 mm and 5 m respectively. In the Z-direction, the domain is extended 1 m upstream of the heated section, so as to allow the solution to establish fully-developed flow profiles at this location.

Boundary conditions are applied at the inlet (Z = 0.0 m), the outlet (Z = 5 m), the tube wall (Y = 0.005 m) and the flow axis (Y=0), which is treated as a symmetry plane. The inlet temperature, T_{in}, is uniform (320 or 350°C) and the inlet turbulence is specified with a turbulence intensity of 5% and a Prandtl mixing length of 10% of the tube radius. At the inlet, a uniform velocity profile, V_{in}, is specified in accordance with the given mass flux, G, and the specified inlet temperature, T_{in}. The outlet of the tube is defined as a fixed pressure boundary. For each modeling case, a uniform heat flux, q, is a specified at the heated section of the outer wall (at $Z >1$ m), and elsewhere the wall is taken as adiabatic.

3.2. Computational details: The model equations are solved numerically using the finite-volume method embodied in the general-purpose PHOENICS CFD code [8]. This method uses a staggered-variable arrangement for the velocity components and scalar variables, and the effects of convection and diffusion are weighted using the hybrid differencing scheme [16]. The solutions of the discretised conservation and turbulence transport equations are obtained using an iterative pressure-correction method based on the SIMPLEST algorithm [17].

The computational grid used for the finite-volume method is uniform in the axial direction and non-uniform in the radial direction. The radial grid is made significantly finer near the tube wall and it expands towards the axis of the tube: a geometric progression distribution with an expansion ratio of -1.08 is used in all the runs for consistency. The number of radial grid cells varied from 40 to 100 and the final runs are made on grids containing 80x400 and 100x400 cells based on grid sensitivity studies.

For all validation runs, the non-dimensional distance from the wall to the first grid node, y^+ is less than unity, which is in accordance with recommendations on the use of low-Re turbulence models in previous CFD analyses of SCW heat transfer [2-7]. In particular, y^+ is around 0.1 in most runs. It is calculated from $y^+=u^*{}_*y_l/v$, where u^* is the friction velocity, y_l is the radial distance from the wall.

The physical property values generated by REFPROP are used to provide a separate MS-Excel table file for each individual property, and these files are then read by the PHOENICS solver at run time. At each computational cell, the physical properties are calculated using linear interpolation to the local temperature value. For simplicity, the PHOENICS customization tool, INFORM [8], is used for linking the PHOENICS solver with the REFPROP data base instead of using FORTRAN coding and creating a private version of the PHOENICS solver.

3.3. Convergence: The convergence requirement is that for each set of finite-volume equations the sum of the absolute residual sources over the whole solution domain is less than 1% of reference quantities based on the total inflow of the variable in question. Additional requirements are that the values of monitored dependent variables at a selected location do not change by more than 0.1% between successive iteration cycles, and that the absolute values of the largest corrections to each variable anywhere in the domain fall to a negligible fraction of the value being corrected. The double-precision solver is employed for better accuracy, as otherwise incomplete convergence was obtained for some cases due to rounding error.

4. RESULTS AND DISCUSSION

4.1 Experimental Conditions: The CFD model described in the previous section is validated using the experimental data obtained at the State Scientific Center of Russian Federation - Institute for Physics and Power Engineering supercritical-test facility (Obninsk, Russia) [9-11]. This set of data was generated within the operating conditions close to those of SCWRs.

Table I summarizes the test conditions for each simulated experiment. The main parameters that differentiate the validation cases are the mass flux, G, the wall heat flux, q, and the inlet temperature T_{in}. In all cases, the operating pressure, P, the inside tube diameter, D, and the heated tube length, L_h, are the same: $P = 24$ MPa, $D = 10$ mm, $L_h = 4$ m. As noted earlier, a turbulent Prandtl number of $\sigma_t = 0.86$ is used for all cases, although for comparison purposes, an additional calculation is made for Case 7 with $\sigma_t = 1.2$.

Table II compares the dimensionless parameters (Re, Gr and Ri) in the two validation cases (Cases 6 and 8). The values of Reynolds number (Re), Grashof number (Gr), and Richardson number (Ri) were estimated using the following equations respectively:

$$\mathrm{Re} = \frac{V_{in} D}{\upsilon_{in}} \quad ; \quad Gr = \frac{\left(1 - \rho / \rho_{in}\right)}{\upsilon_{in}^2} gD^3 \quad ; \quad Ri = Gr / \mathrm{Re}^2 \tag{9}$$

where D is the tube diameter, V_{in} is the inlet velocity, and υ_{in} is the molecular kinematic viscosity at the inlet; ρ_{out} is the minimum density at the outlet, ρ_{in} is the density at the inlet, and g is the gravitational acceleration ($g = 9.81$ m/s^2). The Richardson number expresses the relative importance of natural to forced convection, and it is closely related to the so-called Jackson buoyancy parameter (Bo=Gr/Re^2.7, but with differing Gr definition) [18] used by some other researchers [19] for assessing whether buoyancy effects impact significantly on the near-wall heat-transfer processes in SCW flow in tubes.

Table I. Validation cases (P=24 MPa, D = 10 mm, L_h = 4 m)

Case	G, kg/m^{2}s	q, kW/m^2	T_{in} , °C
1	1500	590	350
2	1500	729	320
3	1000	387	320
4	1000	581	350
5	1000	681	350
6	500	141	350
7	500	334	350
8	200	129	350

Table II. Comparison of parameters in Cases 6 and 8

Parameters	Case 6	Case 8
V_{in}, m/s	0.81	0.32
ρ_{in}, kg/m^3	621.2	621.2
ρ_{out}, kg/m^3	197.5	101.4
Re	6.94·10^4	2.76·10^4
Gr	4.97·10^8	6.10·10^8
Ri	0.10	0.80

4.2 CFD Model Validation: The bulk fluid temperature, the inside tube wall temperature and the heat transfer coefficient are calculated along the heated tube length and compared with experimental data in Cases 1 to 8 listed in Table I. Figures 1-9 show the comparisons of CFD predictions (solid lines) of bulk fluid temperature, inside tube wall temperature and heat transfer coefficient with experimental values (dots).

In the first six cases considered in this paper (Cases 1 to 6), the agreement is very good along the whole tube length (see Figures 1-6 for more details). The blue lines/dots show the predicted/measured bulk-fluid temperature (T_b). The average T_b values obtained from the CFD (solid lines) precisely match the experimental values, as shown in Figures 1-6. Also, the red dots and red solid lines representing the inside tube temperature T_w are close enough. However, some experimental points were not perfectly fitted to the CFD results. In particular, in Case 6 (see Figure 6), we have possibly a number of faulty signals from thermocouples at the axial locations of about 1.5 m, 2 m and close to 4 m.

In Case 7, the quantitative disagreement between the predictions of tube wall temperature and heat transfer coefficient and their experimental values becomes more significant (see Figure 7). This difference decreases with an increase in Pr_t from 0.86 to 1.2 (see Figure 8). The predictions obtained with $Pr_t = 1.2$ agree well with experimental data over the whole heated tube length except in the immediate vicinity of an axial location of 0.5 m. At this location, a local DHT regime is observed experimentally. This regime is characterized by an unexpected local drop in HTC values and a corresponding local rise in the tube wall temperature. It is not predicted by the current CFD model.

In Case 8 (G=200 kg/m^{2}s), the disagreement between predictions and measurements increases further. Figure 9 shows a comparison of CFD results with experimental data in this case. It is seen that there is a good agreement between the predictions and the experimental data within the heated tube length from 0 to 0.5 m and from 3 to 4 m, where we have the normal HT regime. However, the prediction of HTC overestimates the experimental HTC values quite significantly within the central part of the test section (at axial locations from 0.5 to 3 m). This disagreement is possibly due to inability of current model to predict the DHT regime observed in this area. The DHT regime can be linked to a separation of a heated wall with low-density fluid (i.e., "gas-like" fluid) (lower HTCs) from high-density fluid (i.e., "liquid-like" fluid) flowing in the core (higher HTCs). Another possible reason for DHT can be a significant effect of buoyancy force on heat transfer in Case 8 ($Ri = 0.8$). However, some other reasons for the DHT regime can exist. Usually, the DHT regime can be eliminated by increasing mass flux as it is seen in Figure 6 corresponding to $G = 500$ kg/m^{2}s (in this case, $Ri = 0.1$) or by decreasing heat flux.

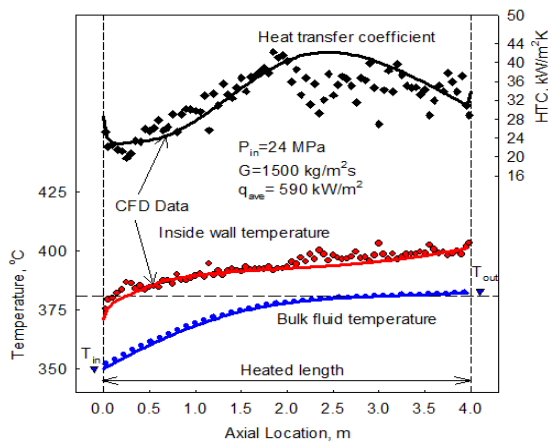**Figure 1 Comparison of CFD Predictions (Solid Lines) with Experimental Data in Case 1 ($G = 1500$ kg/m^{2}s, $q = 590$ kW/m^2).**
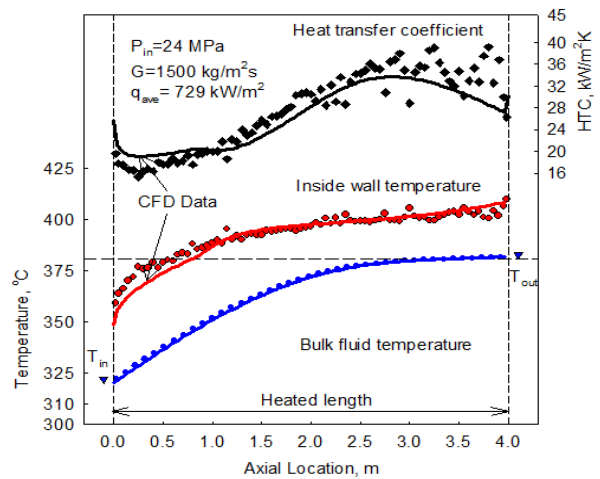

Figure 2 Comparison of CFD Predictions (Solid Lines) with Experimental Data in Case 2 ($G = 1500$ kg/m^{2}s, $q = 729$ kW/m^2).

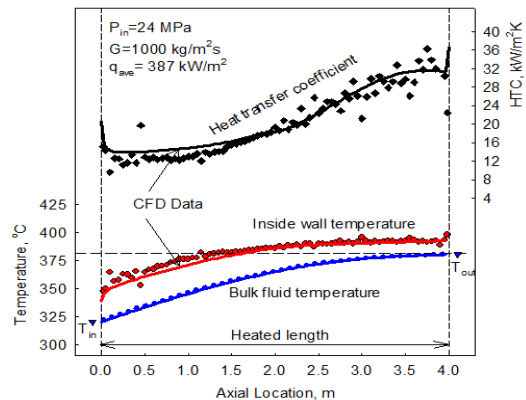**Figure 3 Comparison of CFD Predictions (Solid Lines) with Experimental Data in Case 3 ($G = 1000$ kg/m²s, $q = 387$ kW/m²).**
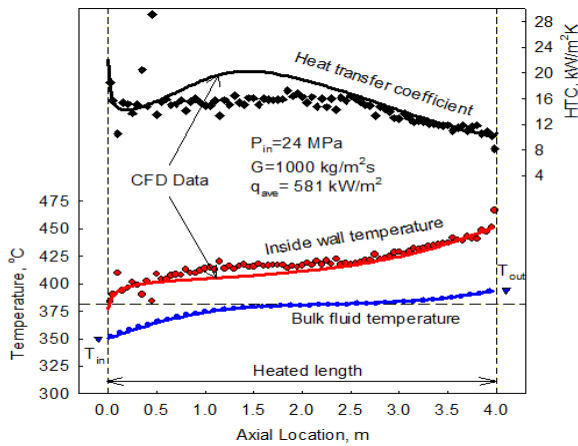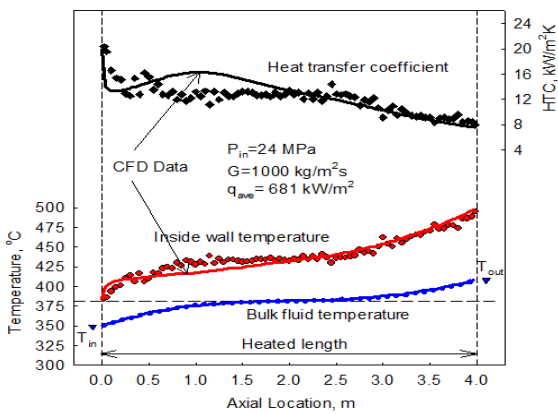

Figure 4 Comparison of CFD Predictions (Solid Lines) with Experimental Data in Case 4 ($G = 1000$ kg/m²s, $q = 581$ kW/m²).

Figure 5 Comparison of CFD Predictions (Solid Lines) with Experimental Data in Case 5 ($G = 1000$ kg/m²s, $q = 681$ kW/m²).
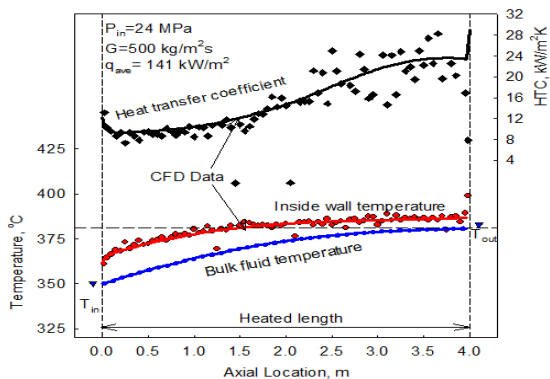
Figure 6 Comparison of CFD Predictions (Solid Lines) with Experimental Data in Case 6 ($G = 500$ kg/m²s, $q = 141$ kW/m²).
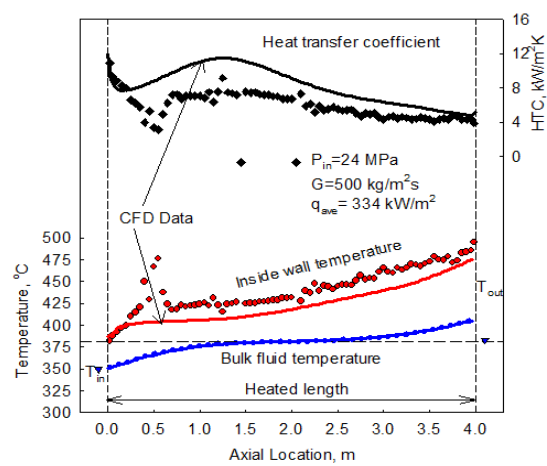
Figure 7 Comparison of CFD Predictions (Solid Lines) with Experimental Data in Case 7 ($G = 500$ kg/m²s, $q = 334$ kW/m²) at $Pr_t = 0.86$.

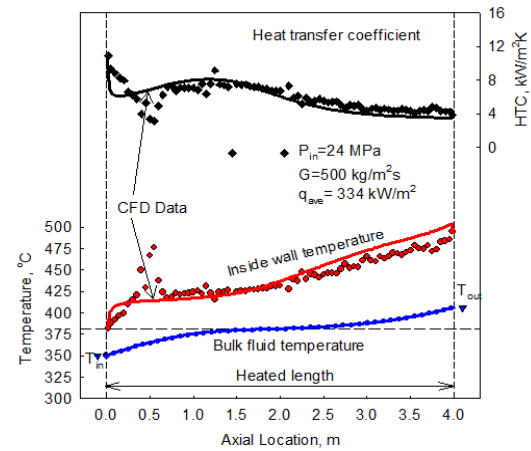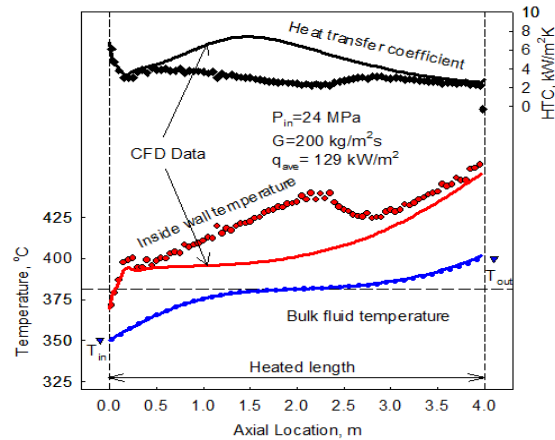**Figure 8 Comparison of CFD Predictions (Solid Lines) with Experimental Data in Case 7 ($G = 500$ kg/m²s, $q = 334$ kW/m²) at $Pr_t = 1.2$.**

Figure 9 Comparison of CFD Predictions (Solid Lines) with Experimental Data in Case 8 ($G = 200$ kg/m^{2}s, $q = 129$ kW/m^2) at $Pr_t = 0.86$

4.3 Flow Characteristics in Cases 5 to 8: Figure 10 shows contour plots of fluid temperature, velocity, density (*DEN1*), laminar kinematic viscosity (*ENUL*), specific heat (*LFCP* in J/kg.K) and laminar Prandtl number (*PRTL*=$\mu C_p/k$) predicted in Case 5 (T_{in}=350°C, G=1000 kg/(m^{2}s), q=681 kW/m^2).

The origin of cylindrical coordinate system is located in the center of inlet tube section (left bottom corner). A red pencil with yellow end (a probe), which is located at the low right corner of the computational domain, shows the center of outlet section. The values of calculated variables at this probe location and their average values in a plane are shown in the high right corners of the figures. For clarity of presentation, the scale in the Y-direction is increased by a factor of 200 in all the figures.

The axial dependence of the laminar Prandtl number is not monotonic: there is a local maximum of about 11.3 in the tube area where the local fluid temperatures are close to the pseudo-critical temperature of 381.2°C, and the specific heat (*LFCP*) reaches the maximum value close to 121.93 kJ/kgK.

In Case 5, the Reynolds number Re=1.39E+5; the Grashof number Gr=6.28E+8; and Richardson number Ri=0.033. This flow is a mixed-convection upward flow in a heated tube, where the buoyancy force caused by density difference becomes important with increase in Ri [20-22]. A detailed review of such flows was provided in [20], where, in particular, it was concluded that the use of low-Reynolds-number turbulence models was required in order to predict accurately the heat transfer characteristics such as tube wall temperature and heat transfer coefficient along the heated tube length.

Due to a large decrease in density (from 621 to about 86 kg/m^3) along the heated tube length, there is a significant acceleration of flow: the velocity increases from an inlet velocity of 1.61 m/s to values up to 8.37 m/s at the tube outlet. Figure 11 shows the dependencies of axial velocity on radial distance from the tube axis predicted in Case 5 at different distances from the tube inlet (1, 2, 3, 4, and 5 m). It is an illustration of significant flow acceleration. However, the effect of buoyancy on radial profiles of axial velocity is not significant in this case (Ri=0.033).

Figure 12 shows the radial profiles of axial velocity in Case 6 (G=500 kg/m^{2}s, q=141 kW/m^2, Ri=0.1). The velocity-profile data were predicted at five different distances from the tube's inlet (1, 2, 3, 4, and 5 m). Due to a large decrease in density (from 621 to about 140 kg/m^3) along the heated tube length, there is a significant acceleration of flow: the velocity increases from an inlet velocity of 0.94 m/s to values up to

1.6 m/s at the tube outlet. As in Case 5, the effect of buoyancy force is negligible: at each axial location, the maximum velocity is predicted at the tube axis (at a radial distance Y=0 m).
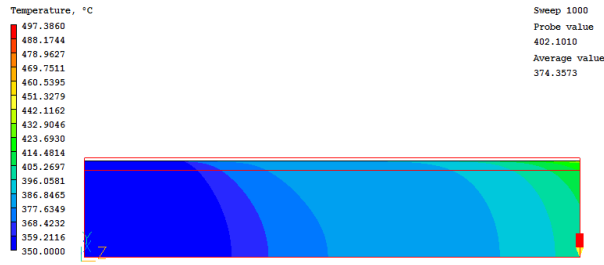
For an increase in Ri, the effect of buoyancy force on fluid velocity and temperature increases and the radial profile of axial velocity starts to have a local maximum between the tube axis and tube wall. This effect was demonstrated in [23] for an ascending air flow in a vertical heated pipe at Re=25,000 and Gr>10^9 (Ri>1.6).

Figure 13 illustrates the above buoyancy effect predicted in Case 7 (T_{in}=350°C, G=500 kg/(m^{2}s), q=334 kW/m^2). This figure shows the radial profiles of axial velocity calculated at different distances from the tube inlet. The modest local maximums (between the tube axis and tube wall) are predicted for radial profiles of axial velocities at the distances of 2 and 3 m from the tube inlet. It is an indication of the moderate local effect of buoyancy on fluid velocity. In this case, Re=6.94E+4, Gr=6.21E+8 and Ri=0.13.
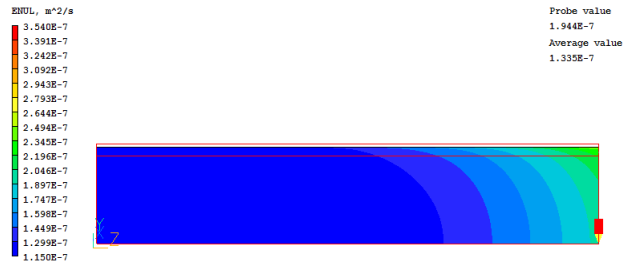
Figure 14 shows the radial profiles of axial velocity in Case 8 (G=200 kg/m^{2}s, Ri=0.8). Due to a significant effect of buoyancy force in this case, these profiles at the axial locations of 2 and 3 m from the tube inlet have local maximums between the tube wall and tube axis. These maximums are not predicted if the buoyancy effect is ignored in the momentum conservation equations (see Figure 15). Comparing Figures 14 and 15 confirms that a special behavior of velocity at 2 and 3 m in Figure 14 is related to the effect of buoyancy force. Additionally, the effect of buoyancy force was studied by plotting the radial profiles of turbulent kinetic energy (TKE) with and without gravitational acceleration. These profiles (at axial distances of 1 and 2 m from tube inlet) are shown in Figures 16 and 17 respectively. The effect of buoyancy force is significant when the gravitational acceleration was accounted for (Figure 16).

For values of the Richardson number, Ri, >0.1, buoyancy will have a significant effect on the near-wall turbulence-transport processes. For the DHT cases 7 and 8, Ri=0.13 and 0.80 respectively, indicating the importance of both natural and forced convection. In practice, under these conditions, there will be a local laminarisation of the flow due a marked reduction in the turbulence production following a modification of the radial distribution of the velocity and turbulent shear stress due to buoyancy, as explained in [22-23]. When the flow rate is reduced or the heat flux is increased sufficiently, the buoyancy force becomes much stronger, accelerating the flow velocity near the heated wall. This leads to a flatter velocity profile, and so the turbulence is suppressed through the reduction in the mean-velocity gradient that appears in the turbulence energy production term P_k. Consequently, this leads to a reduction in the HTC and an increase in the wall temperature.
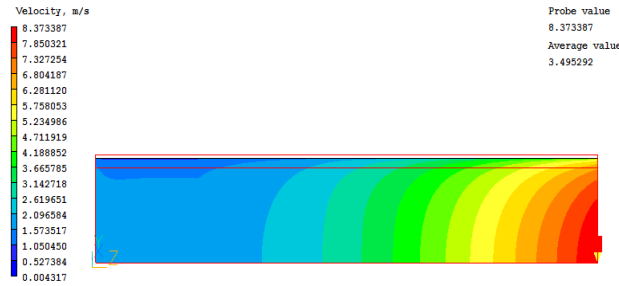
For Cases 1 to 6, the model predictions provide a good match with the measurements, but for the DHT Cases 7 and 8 the model underestimates the wall temperature over most of the tube length and fails to capture the abrupt DHT regions. The disagreement for Cases 7 and 8 is believed to be largely due to the fact that under these mixed-convection conditions, the 2-layer turbulence model produces insufficient damping of the turbulence in the near-wall region, with the result that the wall temperatures are underestimated along most of the tube length. The model does reduce the turbulence significantly for Case 8 as compared to Case 6, as may be established by examining contour plots of the turbulence distortion ratio (P_k/ε) and the local turbulent Reynolds number (v_t/v). However, the turbulence isn't damped enough, which means that using a constant eddy-viscosity coefficient $c_\mu c_d$ is likely to be unsatisfactory under these conditions. Therefore, a more sophisticated representation of the near-wall turbulence processes is required, such as for example by making both v_t and the turbulent Prandtl number functions of both turbulence and buoyancy parameters, and then including buoyancy terms in the k and ε equations, but with the vertical turbulent heat flux computed from an implicit algebraic heat flux model derived from a second moment turbulence closure.
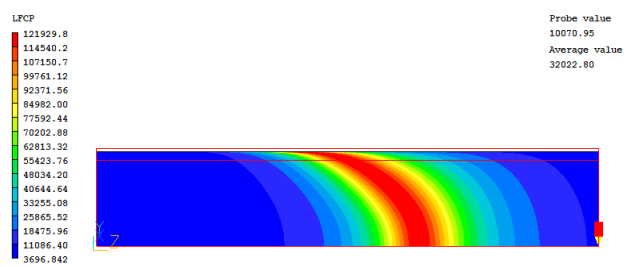
Temperature, °C

497.3860
488.1744
478.9627
469.7511
460.5395
451.3279
442.1162
432.9046
423.6930
414.4814
405.2697
396.0581
386.8465
377.6349
368.4232
359.2116
350.0000

Sweep 1000
Probe value
402.1010
Average value
374.3573

SCWF(2-lk-e,Prt=0.86,100x400:q=681kW/m2

ENUL, m^2/s

3.540E-7
3.391E-7
3.242E-7
3.092E-7
2.943E-7
2.793E-7
2.644E-7
2.494E-7
2.345E-7
2.196E-7
2.046E-7
1.897E-7
1.747E-7
1.598E-7
1.449E-7
1.299E-7
1.150E-7

Probe value
1.944E-7
Average value
1.335E-7

SCWF(2-lk-e,Prt=0.86,100x400:q=681kW/m2

Velocity, m/s

8.373387
7.850321
7.327254
6.804187
6.281120
5.758053
5.234986
4.711919
4.188852
3.665785
3.142718
2.619651
2.096584
1.573517
1.050450
0.527384
0.004317

Probe value
8.373387
Average value
3.495292

SCWF(2-lk-e,Prt=0.86,100x400:q=681kW/m2

LFCP

121929.8
114540.2
107150.7
99761.12
92371.56
84982.00
77592.44
70202.88
62813.32
55423.76
48034.20
40644.64
33255.08
25865.52
18475.96
11086.40
3696.842

Probe value
10070.95
Average value
32022.80

SCWF(2-lk-e,Prt=0.86,100x400:q=681kW/m2

DEN1, kg/m^3

621.1500
587.6881
554.2262
520.7643
487.3024
453.8404
420.3785
386.9166
353.4547
319.9928
286.5309
253.0689
219.6070
186.1451
152.6832
119.2213
85.75934

Probe value
144.5412
Average value
396.7263

SCWF(2-lk-e,Prt=0.86,100x400:q=681kW/m2

PRTL

11.27422
10.63697
9.999722
9.362473
8.725223
8.087974
7.450724
6.813475
6.176225
5.538976
4.901726
4.264477
3.627228
2.989978
2.352729
1.715479
1.078230

Sweep 1000
Probe value
1.958435
Average value
3.689667

SCWF(2-lk-e,Prt=0.86,100x400:q=681kW/m2

Figure 10 Predicted 2D Contours of Temperature, Velocity, Density, Laminar Kinematic Viscosity, Specific Heat and Laminar Prandtl Number in Case 5 (T_{in}=350°C, G=1000 kg/m^{2}s, q=681 kW/m^2).
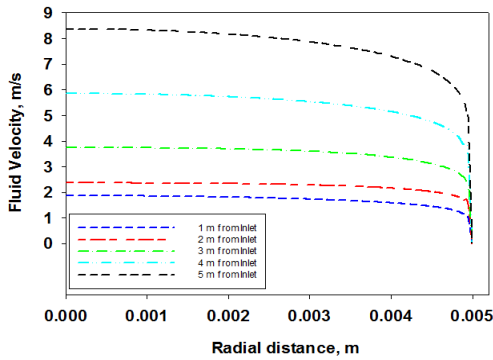
Figure 11 Predicted Radial Profiles of Axial Velocity at Various Distances from the Tube Inlet in Case 5 (T_{in}=350°C, G=1000 kg/m²s, q=681 kW/m²).

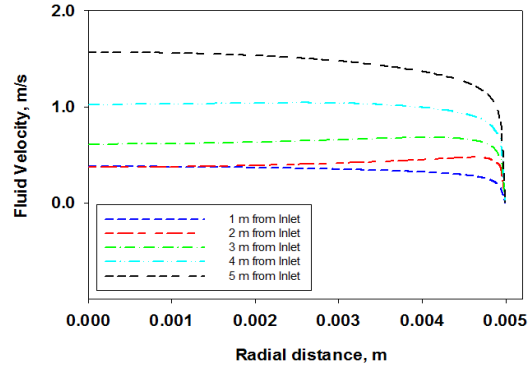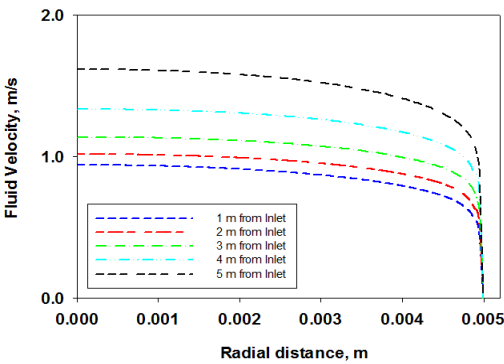**Figure 14 Predicted Radial Profiles of Axial Velocity at Various Distances from the Tube Inlet in Case 8 (T_{in}=350°C, G=200 kg/m²s, q=129 kW/m²).**

Figure 12 Predicted Radial Profiles of Axial Velocity at Various Distances from the Tube Inlet in Case 6 (T_{in}=350°C, G=500 kg/m²s, q=141 kW/m²).
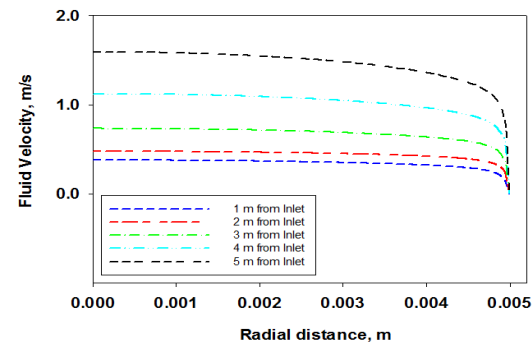

Figure 15 Radial Profiles of Axial Velocity at Various Distances from the Tube Inlet Predicted in Case 8 (T_{in}=350°C, G=200 kg/m²s, q=129 kW/m²) without Considering the Effects of Buoyancy Force.
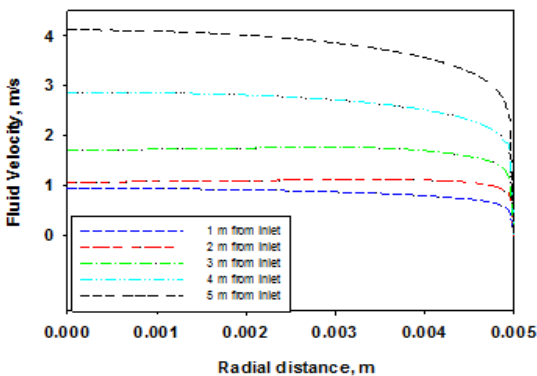

Figure 13 Predicted Radial Profiles of Axial Velocity at Various Distances from the Tube Inlet in Case 7 (T_{in}=350°C, G=500 kg/m²s, q=334 kW/m²).

Figure 16 Radial Profiles of Turbulent Kinetic Energy (TKE) at 1 and 2 m from the Tube Inlet Predicted in Case 8 (T_{in}=350°C, G=200 kg/m²s, q=129 kW/m²) with Considering the Effects of Buoyancy Force.
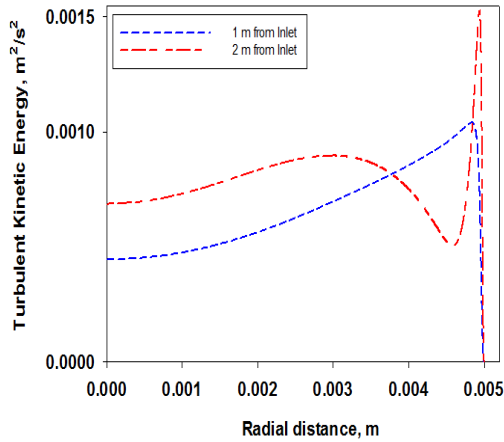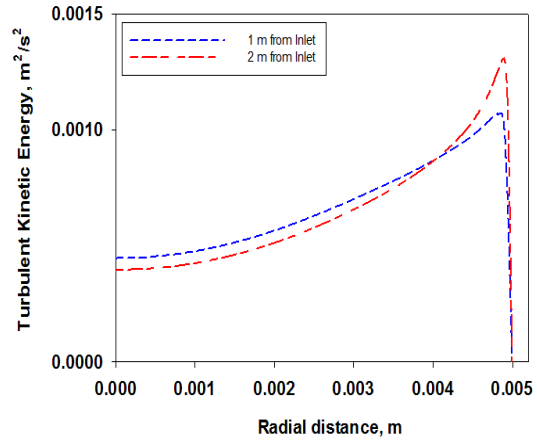
Figure 17 Radial Profiles of Turbulent Kinetic Energy (TKE) at 1 and 2 m from the Tube Inlet Predicted in Case 8 (T_{in}=350°C, G=200 kg/m²s, q=129 kW/m²) without Considering the Effects of Buoyancy Force

5. CONCLUSIONS

The commercial general-purpose CFD software, PHOENICS 2014, has been customized and validated for modeling the SCW heat transfer in a vertical tube upward flow under the operating conditions typical to SCWRs: a pressure of 24 MPa, an inner tube diameter of 10 mm, an inlet temperature of 320 or 350°C, a heated tube length of 4 m, the three values of mass flux (500, 1000 and 1500 kg/m²s) and various values of wall heat flux (from 141 to 729 kW/m²).

The two-layer low-Reynolds-number k-ε model has demonstrated a good performance provided that a turbulent Prandtl number of 0.86 is fixed and the non-dimensional wall distance y^+ is kept below unity.

The study has shown a good agreement between the CFD predictions and the experimental data on the inside wall temperature and heat transfer coefficient in most validation cases. No model tuning is made for validation purposes within a wide range of flow conditions.

A further model development is required under the conditions of low values of mass flux, G, so as to predict accurately the inside tube wall temperature and heat transfer coefficient. For these cases (Cases 7 and 8), the effects of buoyancy forces on the near-wall heat transfer processes becomes significant, and the accuracy of the wall-heat-transfer predictions becomes much less satisfactory.

The partially validated CFD model of SCW heat transfer in a vertical upward tube flow is recommended for practical 3D geometries under the conditions of moderate effects of buoyancy (moderate values of Richardson number).

NOMENCLATURE

C_p Specific heat at constant pressure, J/kg·K
D Inner tube diameter, m
DEN1   Density, kg/m³

ENUL   Laminar kinematic viscosity, m^2/s
G   Mass flux, kg/m^2s
HTC   Heat transfer coefficient, $kW/m^2 \cdot K$
k   Thermal conductivity, $W/m \cdot K$
L   Length, m
LFCP   Specific heat, J/kgK
P   Pressure, Pa
q   Wall heat flux, kW/m^2
T   Temperature, °C
V   Velocity, m/s

Greek Letters
v   Molecular kinematic viscosity, m^2/s
ρ   Density, kg/m^3
μ   Molecular dynamic viscosity, Pa s

Dimensionless Numbers
Gr   Grashof number $((1-\rho_{out}/\rho_{in})gD^3/v_{in}^2)$
PRTL Laminar Prandtl number $(\mu C_p/k)$
Pr_t Turbulent Prandtl number
Re   Reynolds number (DV_{in}/v_{in})
Ri   Richardson number (Gr/Re^2)

Subscripts
h   heated
in   inlet
out   outlet

Abbreviations
CFD   Computational Fluid Dynamics
SCW   SuperCritical Water
SCWRs   SuperCritical Water Reactors
NIST   National Institute of Standards and Technology

ACKNOWLEDGEMENT

REFERENCES

1. Versteeg, H.K., and Malalasekera, W., *An introduction to computational fluid dynamics*, Longman, Harlow, UK (1995).
2. Roelofs, F., *CFD analysis of heat transfer to supercritical water flowing vertically upward in a tube*, Under the contract of the Netherlands Ministry of Economic Affairs (2004).
3. Cheng, X., Kuang, B., and Yang, Y.H., "Numerical analysis of heat transfer in supercritical water cooled flow channels," *Nuclear Engineering and Design*, **237**, pp. 240-252 (2007).
4. Mokry, S., Farah, A., King, K., Gupta, S., Pioro, I., and Kirillov, P., "Development of supercritical water heat-transfer correlation for vertical bare tubes," *Proc. International Conference on Nuclear Energy for New Europe 2009,* Bled, Slovenia, September 14-17, pp. 210.1-210.13 (2009).

5. Vanyukova, G., Kuznetsov, Yu., Loninov, A. et al., "Application of CFD-Code to Calculations of Heat Transfer in a Fuel Bundle of SCW Pressure-Channel Reactor," *Proc. 4th Int. Symp. on Supercritical Water-Cooled Reactors,* March 8-11, Heidelberg, Germany, Paper No. 28, 9 pages (2009).

6. Jaromin, M. and Anglart, H., "A Numerical Study of the Turbulent Prandtl Number Impact on Heat Transfer to Supercritical Water Flowing Upward under Deteriorated Conditions," Proc. 15th International Topical Meeting on Nuclear Reactor Thermal hydraulics (NURETH-15), May 12–17, Pisa, Italy, paper #134, 14 pages (2013).

7. Farah, A., Harvel, G., and Pioro, I., "Assessment of FLUENT CFD Code as an Analysis Tool for Supercritical-Water Heat- Transfer Applications," *Proc. 15th International Topical Meeting on Nuclear Reactor Thermal hydraulics (NURETH-15)*, May 12–17, Pisa, Italy, paper #118, 13 pages (2013).

8. "PHOENICS On-Line Information System," www.cham.co.uk/ChmSupport/polis.php. (2015).

9. Kirillov, P., Pometko, R., Smirnov, A. et al., "Experimental Study on Heat Transfer to Supercritical Water Flowing in 1- and 4-m-Long Vertical Tubes," *Proc. GLOBAL'05*, Tsukuba, Japan, Oct. 9-13, Paper No. 518 (2005).

10. Pioro, I.L., Kirillov, P.L., Mokry, S.J. and Gospodinov, Y.K., "Supercritical Water Heat Transfer in a Vertical Bare Tube: Normal, Improved and Deteriorated Regimes," *Proc. ICAPP'08*, Anaheim, CA, USA, June 8-12, Paper #8333, pp. 1843-1852 (2008).

11. Gospodinov, Ye., Mokry, S., Pioro, I. and Kirillov, P.L., "Supercritical Water Heat Transfer in a Vertical Bare Tube," *Proc. ICONE-16*, Orlando, Florida, USA, May 11–15, Paper #48546, 11 pages (2008).

12. Pioro, I. and Duffey, R., Heat Transfer and Hydraulic Resistance at Supercritical Pressures in Power Engineering Applications, ASME Press, New York, NY, USA, 334 pages (2007)."

13. Rodi, W.,"Experience with two-layer models combining the k-ε model with a one-equation model near the wall," *AIAA-91-0216, 29th Aerospace Sciences Meeting*, January 7-10, Reno, Nevada, USA (1991).

14. Malin, M.R., "On the Calculation of Heat Transfer Rates in Fully Turbulent Wall Flows," *Appl. Math. Modelling*, **11**, pp. 281-284 (1987).

15. National Institute of Standards and Technology, *NIST Reference Fluid Thermodynamic and Transport Properties-REFPROP*. NIST Standard Reference Database 23, Ver. 8.0. Boulder, CO, U.S.: Department of Commerce (2007).

16. D.B.Spalding, "A novel finite-difference formulation for differential expressions involving both first and second derivatives", *Int.J.Num.Meth.Eng.,* Vol.4, p551, (1972).

17. D.B. Spalding, "Mathematical modelling of fluid-mechanics, heat-transfer and chemical-reaction processes, Lecture 25, Improved procedures for Hydrodynamic problems", *CFDU Report HTS/80/1*, Imperial College, London, (1980).

18. J.D. Jackson, & W.B. Hall, "Forced Convection Heat Transfer to Fluids at Supercritical Pressure", Turbulent Forced Convection in Channels and Bundles", Hemisphere Publishing Corporation, New York, 563-611, (1979).

19. Z. Li, Y.Wu, J. Lu, D.Zhang & H.Zhang, "Heat transfer to supercritical water in circular tubes with circumferentially non-uniform heating", Applied Thermal Engineering 70, 190-200, (2014).

20. Jackson, J.D., Cotton, M.A. and Axcell, B.P., "Studies of Mixed Convection in Vertical Tubes," *Int. J. Heat and Fluid Flow*, **10** (1), pp. 2-15 (1989).

21. Abdelmeguid, A.M., and Spalding, D.B., "Turbulent flow and heat transfer in pipes with buoyancy effects," *J. Fluid Mech.*, **94**, pp. 383-400 (1979).

22. Hall, W.B., and Jackson, J.D., "Laminarisation of a turbulent pipe flow by buoyancy forces," *ASME*, Paper No. 69-HT-55 (1969).

23. J.D. Jackson, "Fluid flow and convective heat transfer to fluids at supercritical pressure", Nuclear Engineering and Design 264, 24–40, (2013).